CANCER GENOMICS & PROTEOMICS *17*: 61-76 (2020)
doi:10.21873/cgp.20168

Therapeutic Efficacy Evaluation of Pegylated Liposome Encapsulated With Vinorelbine Plus ^{111}In Repeated Treatments in Human Colorectal Carcinoma With Multimodalities of Molecular Imaging

YI-CHUN CHIEN[1,2*], YING-HSIANG CHOU[3,4*], WEI-HSUN WANG[5,6], JOHN CHUN-HAO CHEN[7], WEN-SHIN CHANG[8], CHIA-WEN TSAI[8], DA-TIAN BAU[8,9] and JENG-JONG HWANG[4,10]

[1]*Department of Medical Imaging and Radiological Sciences, I-Shou University, Jiaosu Village, Kaohsiung, Taiwan, R.O.C.;*
[2]*School of Medicine, I-Shou University, Jiaosu Village, Kaohsiung, Taiwan, R.O.C.;*
[3]*Department of Radiation Oncology, Chung Shan Medical University Hospital, Taichung, Taiwan, R.O.C.;*
[4]*Department of Medical Imaging and Radiological Sciences, Chung Shan Medical University, Taichung, Taiwan, R.O.C.;*
[5]*Department of Orthopedic Surgery, Changhua Christian Hospital, Changhua, Taiwan, R.O.C.;*
[6]*Department of Medical Imaging and Radiology, Shu-Zen Junior College of Medicine and Management, Kaohsiung, Taiwan, R.O.C.;*
[7]*Department of Radiation Oncology, Mackay Memorial Hospital, New Taipei City, Taiwan, R.O.C.;*
[8]*Graduate Institute of Biomedical Sciences, China Medical University, Taichung, Taiwan, R.O.C.;*
[9]*Department of Bioinformatics and Medical Engineering, Asia University, Taichung, Taiwan, R.O.C.;*
[10]*Department of Medical Imaging, Chung Shan Medical University Hospital, Taichung, Taiwan, R.O.C.*

Abstract. *Background/Aim: In precision therapy, liposomal encapsulated chemotherapeutic drugs have been developed to treat cancers by achieving higher drug accumulation in the tumor compared to normal tissues/organs. Materials and Methods: We developed a novel chemoradiotherapeutic approach via nanoliposomes conjugated with vinorelbine (VNB) and ^{111}In (^{111}In-VNB-liposome) and examined their pharmacokinetics, biodistribution, maximum tolerance dose, and toxicity in a NOD/SCID mouse model. Results: Pharmacokinetic results showed that the area under the curve (AUC) of PEGylated liposomes was about 17-fold higher than that of the free radioisotope. Tumor growth inhibition by ^{111}In-VNB-liposome was significantly higher than that of the control ($p<0.05$). Conclusion: The tumors in NOD/SCID mice bearing HT-29/tk-luc xenografts were significantly suppressed by ^{111}In-VNB-liposomes. The study proposed repeated treatments with a novel liposome-mediated radiochemotherapy and validation of therapeutic efficacy via imaging.*

*These Authors contributed equally to this study.

Correspondence to: Jeng-Jong Hwang, Ph.D., Professor, Department of Biomedical Imaging and Radiological Sciences, National Yang-Ming University No. 155, Sec. 2, Li-Nong St., Beitou, Taipei 112, Taiwan, R.O.C. Tel: +886 228267064; Fax: +886 228201095, e-mail: jjhwang@ym.edu.tw; johnjjhwang@gmail.com; Da-Tian Bau, Terry Fox Cancer Research Laboratory, Translational Medicine Research Center, China Medical University Hospital, 2 Yuh-Der Road, Taichung, 404 Taiwan, R.O.C. Tel: +886 422053366 (Ext. 5805), e-mail: datian@mail.cmuh.org.tw; artbau2@gmail.com

Key Words: Biodistribution, bioluminescence, colorectal cancer, PEG-liposome, pharmacokinetics, micro positron emission tomography.

Colorectal cancer is a common malignant tumor in industrialized countries (1-3). From an epidemiological viewpoint, family inheritance, ageing and diabetes may all contribute to a higher risk of colorectal cancer (4-6). Clinically, colorectal cancer has a high mortality rate due to the fact that it remains undetected until later stages of the disease (7). The average five-year overall survival rate for all stages is about 65% based on surgery, adjuvant chemotherapy and radiotherapy (8).

Vinorelbine (5'-noranhydrovinblastine, VNB) is a drug widely used in cancer therapy (9, 10). It acts through microtubule disruption, thereby arresting cell division in mitosis. Also, it is less toxicity than the naturally occurring

vinca alkaloids (11, 12). Today, patients receive chemotherapy mainly orally or intravenously. However, these means of administration result in the exposure of all organs of the body and the tumor to the same concentration of the drug, giving the drug a chance to damage the normal tissues. Thus, there is need to accurately and effectively deliver the drug to the lesion, as with radiation therapy.

The development of radiation therapy has advanced rapidly in recent years. Radionuclide therapy differs from traditional radiotherapy, since it delivers radioisotopes directly into the body's lesions. This methodology, is beneficial for the patients not only due to the shortening of the treatment time, but also due to the improved normal tissue/organ tolerance. Indium-111 (^{111}In) is a radioactive isotope of indium (In) with an appropriate half-life ($T_{1/2}$=2.8 days). During its decay by electron capture (EC) to ^{111}Cd, the released gamma photons can be imaged using planar or SPECT (single photon emission computed tomography) gamma camera (γ-camera). Simultaneously the emitted Auger electrons produce a cancer therapeutic effect with high linear energy transfer (13). Several studies have reported that ^{111}In-labeled drugs can be very effective in cancer therapy and can be used for real-time tracking of drug biodistribution (14-16).

Liposomes, usually 50-500 nm in diameter, are small artificial spherical vesicles with both hydrophobic and hydrophilic characteristics. Liposome-based chemotherapeutic drugs have been shown to increase the stability of the drug *in vivo*, extend the duration of drug retention in the blood circulation, and accumulate the drug at the tumor site. Therefore, liposomes can reduce the possible side effects of chemotherapy drugs on normal tissues and organs and improve therapeutic efficacies (17-19). The modification of the liposome phospholipids with polyethyleneglycol (PEG), usually named PEGylated liposomes, reduce the chance of the liposome to be captured by macrophages in the reticuloendothelial system (RES), and extend the time that the liposomes circulate in blood vessels (20-22). The characteristics and advantages of liposomes have been reported in several studies indicating that they significantly improve biodistribution and therapeutic efficacy of specific drugs (23, 24). In defining a therapeutic strategy, prospective anti-tumor drugs are designed to improve tumor growth control while reducing damage to normal tissues and organs as well (25-27). The enhanced permeability and retention (EPR) effects observed in many types of cancer are most commonly used for passive targeting. The main cause of EPR is the rapid growth of tumor tissue and vigorous angiogenesis. The liposomes can utilize the characteristics of tumor cells to carry radiotherapy and chemotherapeutic drugs in the tumor, where they enter the cells by endocytosis improving the therapeutic effects, protecting normal tissues while killing tumor cells (28-30).

Reporter gene technology is widely used in molecular biology. The herpes simplex virus-1-thymidine kinase (HSV1-*tk*) gene has been used as a suicide gene in cancer therapy for more than 25 years. However, it is more known for its contribution to non-invasive imaging, both clinically and preclinically, using positron emission tomography (PET) for tracking the growth of tumors (31-33). Another renowned reporter gene is the luciferase (*luc*) gene. Firefly luciferase reacts with firefly luciferin (LH_2) (a substrate of luciferase) in the presence of ATP-Mg^{2+} to produce inorganic pyrophosphate and intermediates, luciferyl-adenylate (LH_2-AMP), followed by LH_2-AMP oxidative decarboxylation that produces oxyluciferin, CO_2, AMP, and green biological luminescence, which can be used to track tumor cell growth and metastasis (34-37). The current study will use human colorectal cancer cell line (HT-29) transfected the double-reporter gene of herpes simplex virus-1-thymidine kinase (HSV1-*tk*) and firefly luciferase (*luc*). The human colorectal cancer cell line HT-29/*tk-luc*, stably expressing this double-reporter gene, will be implanted into NOD/SCID mice to establish an animal model for examining the therapeutic efficacy evaluation of a novel combination of VNB plus ^{111}In.

In addition, to validate the established therapeutic efficacy evaluation system, we will examine the efficacy of the novel radiochemotherapy of VNB plus ^{111}In, and investigate its pharmacokinetics, biodistribution, maximum tolerated dose, radiation dose and drug toxicity of ^{111}In-VNB-liposome. The evaluation platform will be used to compare the efficacy of the combined treatment with radiopharmaceuticals plus VNB *versus* radiopharmaceutical alone or VNB alone as well as the efficacy of the repeated dose with that of the single dose. The therapeutic efficacy evaluation platform, the combination treatment and repeated treatments may be used concurrently with radiotherapy in clinical practice against colorectal carcinomas.

Materials and Methods

Tumor cell preparation. The human colorectal cancer tumor cells (HT-29/tk-luc colorectal carcinoma cell line) were maintained in RPMI-1640 medium (Gibco, Grand Island, NY, USA) with 10% heat-inactivated fetal bovine serum (FBS) (Hyclone, Logan, UT, USA) and supplemented with L-glutamine, sodium bicarbonate, 100 units/ml penicillin and 100 μg/ml streptomycin at 37˚C with 5% CO_2 in the presence of 500 μg/ml G418 (Merck, Branchburg, NJ, USA) in order to maintain stable expression of the reporter genes.

Tumor xenografted animal model. Tumor cells (2×10^6 cells/200 μl) were transplanted subcutaneously into the dorsal region of the right thigh of 6-week-old male NOD/SCID (with T- and B-cell deficiency, purchased from National Taiwan University Hospital Animal Center, Taipei, Taiwan) and this was followed by daily measurement using a digital caliper once the tumor bulge caused by the tumor cells at the injection site was visible. Fourteen days after inoculation tumors were assessed twice per week for one month,

and when tumor size reached about 100±5 mm^3, they were treated with or without ^{111}In-VNB-liposomes. Tumor volume was calculated using the formula: =0.523×(length×width×thickness).

Transfection of the double reporter gene tk-luc into human colorectal cancer cell line. The HT-29 parental cells were cultured in 10 cm culture dishes. Five μg pC1-*tk*-IRES-*luc* plastid and 10 ml jetPEI reagent (Polyplus-transfection, Strasbourg, France) were added to 250 ml NaCl solution (150 mM). The two solutions were then mixed and placed at room temperature for 30 min to give a DNA-cationic complex. This mixture was added to HT-29 parental cells and cultured for 24 h for transfection. The transfected cells were selected using 500 μg/ml G418 (Merck) for two weeks. The expression of the *luc* gene was measured in a Wallac 1420 Multilabel Counters (PerkinElmer Life and Analytical Sciences, Wallac, Turku, Finland). The transfected cells (HT-29/*tk-luc*) were sub-cultured for 10 generations to confirm that the reporter gene was stably expressed. HT-29/*tk-luc* cells were cultured under the same conditions as the parental HT-29 cells in medium containing 200 μg/ml G418 (Merck) to maintain the stable expression of the *tk/luc* gene.

Preparation of PEGylated liposomes. The preparation of the PEGylated liposomes was performed as previously described by Tseng *et al*. (38). Briefly, 0.9 mol% of PEG-distearoylphosphatidylethanolamine (DSPE) were prepared at the following ratios: disteroylphosphatidylcholine (DSPC): cholesterol (Chol): DSPE covalently linked polyethylene glycol (PEG) of 2:1:0.027. Small unilamellar vesicles (SUV, ~100 nm diameter) were produced by a combination of the standard thin-film hydration method, the freeze and thaw method and repeated extrusion. The extra-liposomal salt was removed by a Sephadex G-50 column and elution with histidine-sucrose buffer (24 mM histidine hydrogen chloride, 90 g/l sucrose, pH adjusted to 6.0 with NaOH).

Anticancer drugs encapsulation. After removing the extra-liposomal salt by a Sephadex G-50 column, the anti-cancer agent, VNB was added immediately into the solution at a concentration of 3.5 mg VNB per 10 μmol phospholipid, and incubated at 60˚C for 30 min on a hot plate magnetic stirrer (Corning) agitated with a stir bar and setting at 100 rpm. After loading, liposomal VNB was sterilized by 0.2-micron filtration and stored at 4-6˚C until use. The PEGylated liposomes were characterized as follows: pH=6.1, osmolality=361 mmol/kg, mean particle size=95.2 nm, phospholipids=6.19 μmol/ml, VNB=2.08 mg/ml.

Radiolabeling of ^{111}In-oxine. The labeling of oxine with ^{111}In was performed as previously described by Chow *et al*. (39). Briefly, 15 μl of 68 mM 8-hydroxyquinoline (oxine; Sigma-Aldrich Co., St. Louis, MO, USA) in ethanol were added to 10 μl of ^{111}In (indium chloride in 0.05 M HCl; 3.7-74 MBq; Perkin Elmer, Boston, MA, USA) in 400 μl of 0.1 M sodium acetate buffer (pH 5.5) and then incubated at 50˚C for 20 min. The lipophilic components were extracted with chloroform and then evaporated. The labeling efficiency of ^{111}In-oxine was determined by an instant thin layer chromatography (ITLC) method. The radiochemical yield was generally greater than 90% ^{111}In-oxine.

Preparation of PEGylated ^{111}In-VNB-liposomes. The extracted ^{111}In-oxine residue was dissolved in 20 μl of ethanol and added to 80 μl of distilled water. The mixture was incubated with 1.5 ml of liposomes for 30 min at 37˚C. EDTA (2 mg) was then added to chelate any residual free indium-111 and to promote prompt excretion after *i.v.* injection. The labeling of ^{111}In within the liposomes (0.9 mol% PEG) was assayed by loading a 100 μl sample onto a column (40×8 mm; Bio-Rad; Hercules, CA, USA) containing Sephadex™ G-50 fine gel and elution was with normal saline. The labeling efficiency was determined by dividing the radioactivity in VNB-liposome fractions by the total amount loaded. The radioactivity of each fraction was measured using either a dose calibrator (CRC-15R, Capintec, Bioscan, Ramsey, NJ, USA) or a gamma scintillation counter (Cobra II Auto-Gamma counter; Packard). The entrapment of indium-111 was more than 90% (39).

Pharmacokinetics of ^{111}In-VNB-liposomes in HT-29/tk-luc tumor-bearing mice. Six-week-old normal mice were randomly divided into experimental group (^{111}In-VNB-liposom) and control group (unencapsulated ^{111}In-DOTA). After intravenous (*i.v.*) administration of radiopharma-ceuticals, blood was collected at 1, 5, 15, 30, 60 min, and 2, 4, 8 h, and then every 4 h until 72 h thereafter. Using a lancet (Assistant, Germany) to make a stab into the mouse cheek, approximately halfway between the ear and the mandible with enough pressure to produce a small incision. Drops of blood excluded from the stick point and were collected into a 1 μl glass capillary. The radioactivity was measured by a gamma scintillation counter, and the amount of drug remaining in the blood at each time point was calculated by the following formula and expressed in terms of injection activity per ml (% ID/ml).

$$\%ID/ml = \frac{A_0 \times 1000}{\text{Injected dose } (\mu Ci) \times 3.7 \times 10^4 \times 60 \times Eff \times \text{blood volume (ml)}}$$

where $\ln(A/A_0) = -0.693t/t_{1/2}$, A=radioactivity of blood sample by γ-counter, A_0=decay-corrected radioactivity of blood sample, $t_{1/2}$=half-life of radioisotope, t=time after injection and Eff is the counting efficiency of the gamma scintillation counter (Eff=0.42).

Biodistribution of ^{111}In-VNB-liposomes in the HT-29/tk-luc tumor-bearing mice. The tumor-bearing mice (tumor size~ 100 mm^3) were intravenously (*i.v.*) administered 3.7 MBq of 0.9 mol% PEG ^{111}In-VNB-liposomes. For the biodistribution studies (*n*=4 per time point), mice were sacrificed at 1, 4, 24, 48 and 72 h post injection. Anatomization was carried out and tissues/organs of interest including blood, heart, lungs, liver, stomach, spleen, pancreas, large and small intestines, bladder, urine, kidneys, muscle, bone marrow and the tumor were excised, the net tissue weights were obtained and the level of radioactivity in each tissue was measured using a gamma scintillation counter at 72 h after injection. The results were expressed as counts per min (cpm) with decay correction standards, and were normalized as percentage of the injected dose per gram of tissue (%ID/g) (40).

$$\%ID/g = \frac{A0 \times 1000}{\text{Injected dose } (\mu Ci) \times 3.7 \times 10^4 \times 60 \times Eff \times \text{organ weight}}$$

Bioluminescence imaging (BLI). BLI was performed using an IVIS50® animal imaging system (Xenogen, Corp., Alameda, CA, USA.). The photons emitted from the target site penetrate through the mammalian tissue and can be externally detected and quantified using a sensitive light-imaging system (39). On day 17 after inoculation (tumor size ~100 mm^3), the mice were anesthetized with 1-3% isoflurane using a vaporizer system and intraperitoneally

injected with 150 mg/kg D-Luciferin 15 min prior to imaging. The image acquisition time was 2 sec. The displayed images of the tumor sites were drawn around and quantified in photons/second (ph/sec) using Living Image software (Xenogen, Corp.).

Single photon emission computed tomography (SPECT). SPECT dynamic images at 4, 24, 48 and 72 h after intravenous injection of ^{111}In-VNB were obtained from three NOD/SCID mice with HT-29/*tk-luc* tumors (with a tumor size of 100 mm^3). Mice were anesthetized with 1-2% isoflurane gas and e.Cam Multiangle Cardiac (Siemens, Munich, Germany) equipped with a 4 mm pinhole for 20 min. The region of interest (ROI) of the tumor and the contralateral thigh muscle of the same size was circled, and the %ID/g of the ROI and the ratio of the radioactivity on both sides were calculated.

Whole-body autoradiography of mice. Mice were subjected to whole-body autoradiography after 48 h of intravenous injection of ^{111}In-VNB-liposome. The mice were sacrificed with carbon dioxide, fixed posture and then rapidly immersed in isopentane (Nacalai Tesque, Kyoto, Japan) as a medium for liquid nitrogen freezing. After the mouse ears, hands, feet and tail were cut off in about 3 to 5 min, they were placed on a cryostat holder (7×5 cm) and the mice were fully covered with 4% carboxylmethycellulose (CMC). The coated sample was quickly placed in cryostat (Bright Instrument, Huntingdon, UK) frozen (–40˚C) for about 30 min. Frozen sections of about 30 μm were prepared and immediately placed on a pre-cooled adhesive tape (Deer brand, Four Pillars Company, Taipei, Taiwan, ROC). Then, they were placed on an imaging plate (IPs) (BAS-SR2040, Fuji Photo Film, Tokyo, Japan) in an imaging plate cassette (2040, Fuji Photo Film) for imaging. The imaging time was three days, and the IPs were finally analyzed with the FLA5000 reader (Fuji Photo Film).

Body weight and survival assessment. Six-week-old NOD/SCID male mice were treated with tumor cells under the skin of the right thigh. When the tumor grew to a size of about 100 mm^3, the animals were divided into four groups of 10 mice each: control group (liposome), radiotherapy group (^{111}In-liposome), chemotherapy group (VNB-liposome), and the combined treatment group (^{111}In-VNB-liposome). The body weight loss and surviving fractions were estimated after a single dose and multiple doses (once a week, for one month) of drug were administered. The body weight change of each mouse was measured twice per week for one month. Survival was monitored daily and continued until all mice were dead post injection. The results were then subjected to Kaplan–Meier survival analysis.

Micro-PET. At the end of the treatment process (forty-eight days after tumor implantation), a total of twelve mice from the control group and each experimental group of three mice were analyzed. Twenty-four h before imaging, each animal was injected with about 50 μCi (1.85 MBq) of ^{124}I-FIAU *via* the tail vein; 1 h before imaging, each animal was injected with 50 μCi (1.85 MBq) of ^{18}F-FEAU *via* the tail vein. Animals were scanned using a PET R4 scanner (Concorde Microsystems, Knoxville, TN, USA) for 10 min and photographed with a steady supply of oxygen and maintained under anesthesia with 2% isofluorane. The 3D stereo image was taken at an energy of 350 to 650 keV. The images of the micro-PET of ^{124}I-FIAU and ^{18}F-FEAU were analyzed by software ASIPro (Concorde Microsystems, Knoxville, TN, USA). In each image, the ROI of the tumor location was circled, and the radioactivity of the region and the injection dose per gram (%ID/g) were calculated.

Biochemistry and hematology analyses. At the completion of the experiments (at the 50th day after tumor implantation), the mice were sacrificed. Blood samples were collected and tested as follows: alkaline phosphatase (ALP), alanine aminotransferase (ALT), aspartate amino-transferase (AST), creatinine (CRE), blood urine nitrogen (BUN) and albumin (ALB). The above measurements were performed on a BECKMAN CX-5 PRO (Diamond Diagnostics, Holliston, MA, USA).

Tissue preparation for histopathology. At the end of the experiments, samples of the tumor mass and the major organs including lungs, liver, spleen and kidneys were fixed in cold 4% paraformaldehyde, embedded in paraffin, sectioned at 5 μm, and stained with hematoxylin and eosin (H&E staining).

Statistical analysis. The *Student's t*-test was used to examine the significance of differences. Statistically significant differences were identified at $p<0.05$ (marked as *) and $p<0.01$ (marked as **).

Results

Evaluation of the stability of HT-29/tk-luc reporter gene expression. First, the expression of *tk-luc* was examined. As shown in Figure 1A and B, the number of cells correlated well with the number of photons detected ($R^2=0.99$) (Figure 1A and B). In addition, the FIAU uptake assay of the thymidine analog labeled with radioactive iodine 131 (Figure 1C) indicated that longer drug treatments were associated with higher accumulation of radioactivity within the cells. At the same time, no absorption of the drug was detected in cells without the *tk* gene, and there was a significant difference between the two groups ($p<0.05$).

Pharmacokinetics of ^{111}In-VNB-liposome in HT-26/tk-luc tumor-bearing mice. Twelve six-week-old healthy SCID mice were randomized into two groups, one group was injected with ^{111}In-VNB-liposome and another group with ^{111}In-DOTA. The detecting time points after administration and %ID/ml are shown in the horizontal and vertical axis, respectively, of Figure 1D. It is clear that the radioisotope in the group without the liposomes is rapidly metabolized in the body compared with that in the group with the liposomes (Figure 1D). The pharmacokinetics were calculated by software Winalin and are presented in Figure 1D and in Table I. The parameters include half-life ($T_{1/2}$), maximum activity time (T_{max}), highest activity (C_{max}), area under the curve ($AUC_{(0-\infty)}$), and Clear rate (CL). The clearance rate of the experimental group (^{111}In-VNB-liposome) was significantly lower than that of the control group (^{111}In-DOTA), and the results were also reflected in the area under curve (AUC). The signal of the experimental group was about 17-fold higher than that of the control group (Table I).

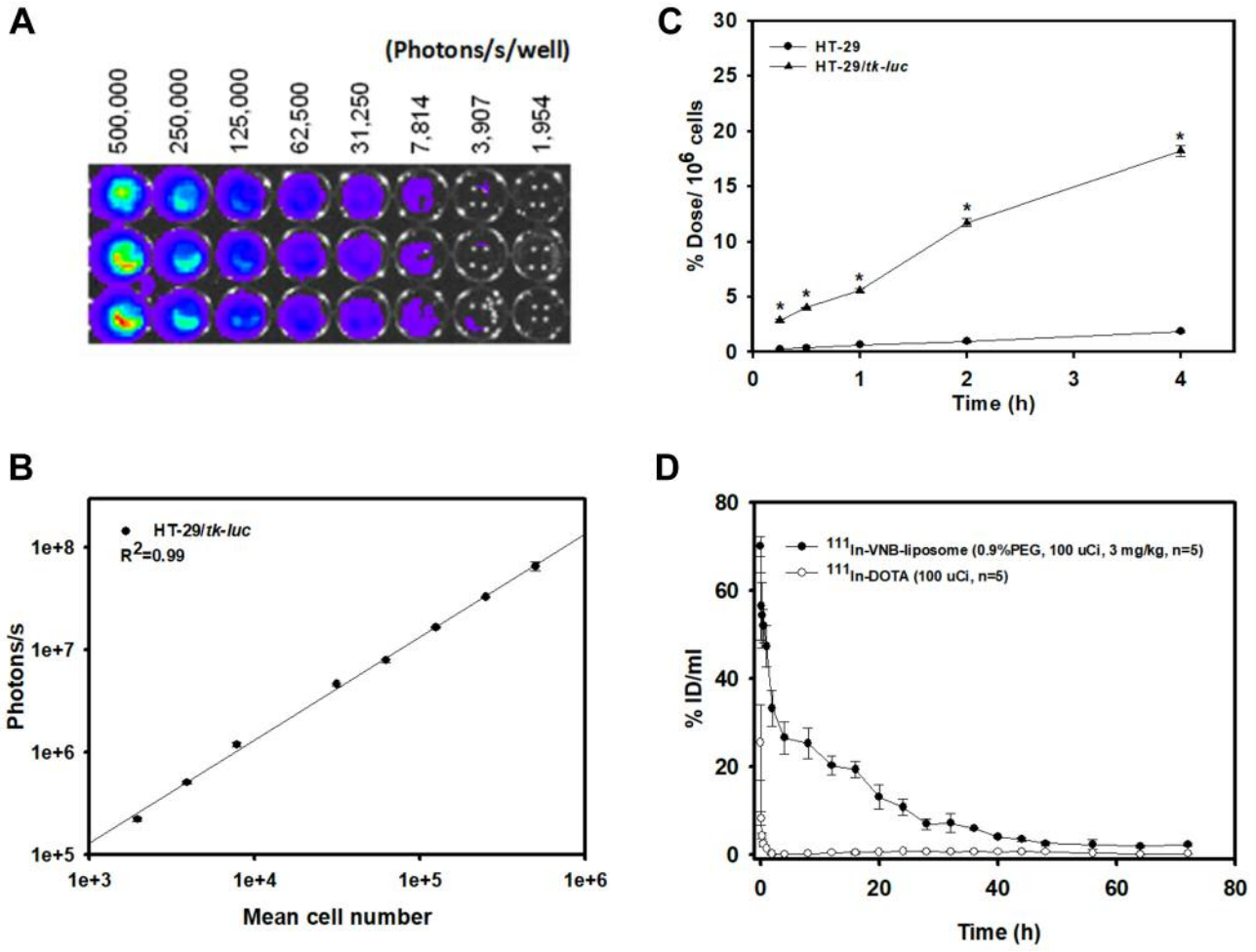

Figure 1. *Evaluation of the stability of HT-29/tk-luc reporter gene expression. (A) The luciferin concentration in each well is 150 μg/ml, and the luminescence image obtained by IVIS50 for 5 sec; (B) A plot of the number of cells versus the total number of photons measured per sec. 5×10^5 cells were serially diluted by a one-half gradient and cultured in 96-well plates; (C) Detection of Herpes simplex virus type 1-thymidine kinase using ^{131}I-FIAU as a probe; (D) Pharmacokinetics of 0.9% PEG 111In-VNB-liposomes in NOD/SCID mice. Pharmacokinetic experiments of ^{111}In-VNB-liposomes and ^{111}In-DOTA in mice.*

Biodistribution of ^{111}In-VNB-liposomes in HT-26/tk-luc tumor-bearing mice. The biodistribution experiments were performed when the tumors were grown up to 100 mm^3 in NOD/SCID mice. Five mice at each time point were sacrificed with carbon dioxide at 1, 4, 24, 48 and 72 h after administration of ^{111}In-VNB-liposome. The radioactivity measured after removal of various organs was calculated as the injection dose per gram (%ID/g) as presented in Figure 2 and summarized in Table II. It can be observed that the amounts of ^{111}In-VNB-liposome in the blood decreased rapidly and time-dependently, and after 24 h, the small intestine, spleen, and liver had a significant accumulation of ^{111}In-VNB-liposome (Figure 2). The highest tumor/muscle ratio fell at 48 h after ^{111}In-VNB-liposome treatment (Table II).

Table I. *The pharmacokinetic parameters of ^{111}In-VNB-liposome and ^{111}In-DOTA.*

Parameter		^{111}In-VNB-liposome	^{111}In-DOTA
$T_{1/2}$	(h)	13.70	0.038
T_{max}	(h)	0.0167	0.0167
C_{max}	(%ID/ml)	70.01	25.54
$AUC_{(0-t)}$	(h*{%ID/ml})	733.00	45.52
$AUC_{(0-\infty)}$	(h*{%ID/ml})	753.96	45.52
Cl	{%ID}/(h*{%ID/ml})	0.122	2.20

Liposomes passively target the tumor as detected with a γ-camera. Compared with other tissues, high radioactivity accumulation in tumors and the liver were observed. We

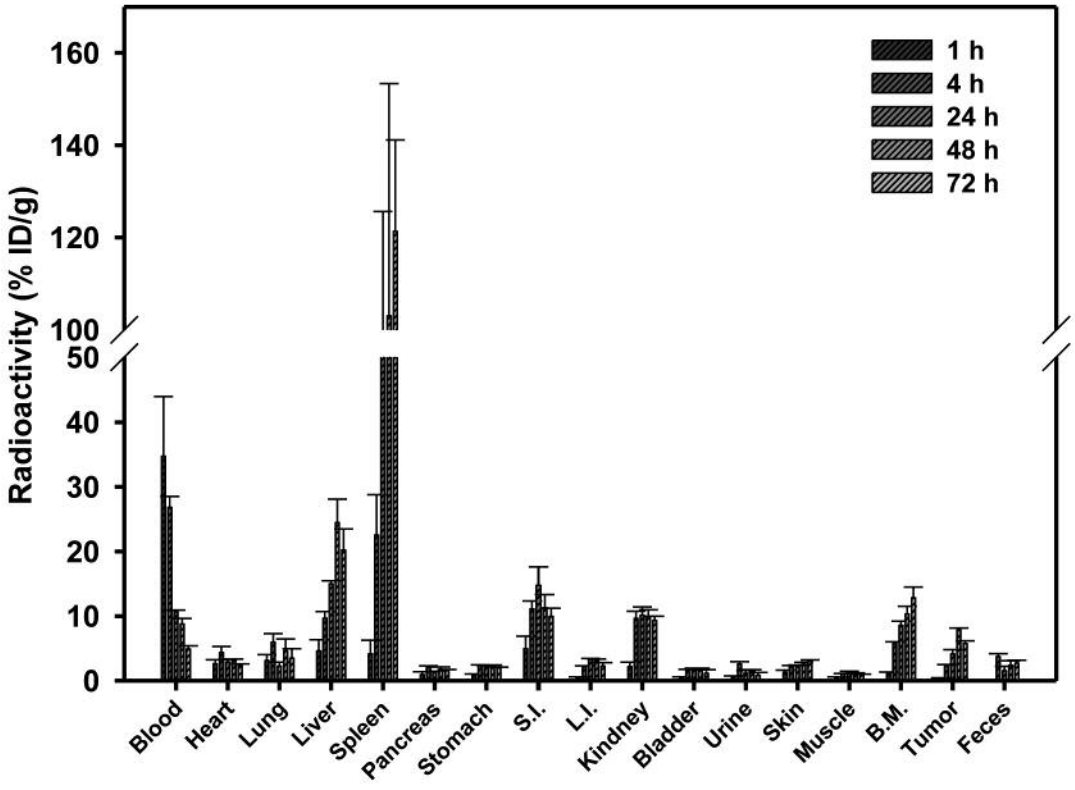

Figure 2. *Biodistribution of ^{111}In-VNB-liposome in HT-29/tk-luc NOD/SCID mouse animal model. One, 4, 24, 48 and 72 h, after the drug ^{111}In-VNB-liposome was administered 5 mice were sacrificed and the radioactivity in various organs was calculated per gram.*

circled and accessed the number of gamma photons per minute (cpm) in Figure 3A, calculated the cumulative radioactivity by the half-life formula and presented the results in Figure 3B. The results showed that the amount of ^{111}In-VNB-liposome gradually increased, reaching a maximum at 48 h after administration (Figure 3B). Similarly, the number of gamma photons of the same ROI size on the opposite side of the tumor was calculated, and the ratio was obtained. The tumor/muscle ratio (T/M ratio) reached its highest value also at 48 h after administration (Figure 3C).

Biodistribution of ^{111}In-VNB-liposomes assayed by whole-body autoradiography. In the previous biodistribution experiments, we obtained the highest ratio of tumor site accumulation to general tissue at 48 h after the administration of the liposome-encapsulated drug. Biodistribution was also examined by whole-body autoradiography at each time point (Figure 4). Optical imaging with a digital camera indicated that the drug obviously accumulated in the liver and small mesentery, which is consistent with the previous biodistribution (Figure 2). At the same time, it was also noticed that the drug accumulated in the tumor location. On the outside of the tumor, the activity near the blood vessels was higher, but not limited to the periphery of the tumor (Figure 4).

^{111}In-VNB-liposome maximum tolerated dose in NOD/SCID mice. To determine the maximum dose that can be administered during treatment, ^{111}In-VNB-liposomes of different radioactivity (0, 300, 400, 500 and 1000 μCi) were injected into the tail vein of NOD/SCID mice. The changes in body weight and survival in mice are depicted in Figure 5A. On the 8th day after drug treatment, the first dead mouse appeared in the group of 1000 μCi, and the best survival rate after four weeks was observed in the 300 μCi group (Figure 5B). Based on the results of survival, it was concluded that the maximum radioactivity that NOD/SCID mice can tolerate for ^{111}In-VNB-liposome (VNB concentration at 3 mg/kg) is 300 μCi.

Weight and tumor size tracking during single-dose therapeutic efficacy assessment. The single-dose treatment began when the tumor grew to a size of 100 mm^3. After three weeks of intravenous drug administration, the tumor size and the body weight of the mice were measured twice

Table II. *Biodistribution of ^{111}In-VNB-liposome in HT-29/tk-luc NOD/SCID model.*

Organ	1 h	4 h	24 h	48 h	72 h
Blood	34.74±9.15	28.82±1.71	10.66±0.28	8.77±0.88	4.91±0.49
Heart	2.63±0.61	4.38±0.92	2.88±0.40	3.02±0.34	2.39±0.21
Lung	3.11±0.94	5.97±1.31	2.27±0.59	4.62±1.86	3.49±1.47
Liver	4.61±1.72	9.69±1.00	15.00±0.47	24.48±3.61	20.24±3.25
Spleen	4.18±2.11	22.55±6.25	97.93±27.70	103.01±50.32	121.33±19.82
Pancreas	0.94±0.45	2.08±0.21	1.32±0.13	1.77±0.36	1.60±0.15
Stomach	0.80±0.25	2.40±0.07	2.10±0.26	2.26±0.17	2.02±0.07
S.I.	4.95±1.93	11.11±1.23	14.76±2.86	11.31±2.03	9.94±1.27
L.I.	0.43±0.15	2.16±0.13	3.34±0.11	3.09±0.26	2.27±0.54
Kidney	2.20±0.66	9.63±1.12	10.11±1.31	9.99±1.00	9.31±0.68
Bladder	0.36±0.22	1.60±0.16	1.67±0.26	1.69±0.24	1.13±0.56
Urine	0.48±0.27	2.59±0.36	1.15±0.42	1.34±0.36	0.83±0.44
Skin	1.28±0.36	2.27±0.08	2.10±0.32	2.52±0.32	3.00±0.22
Muscle	0.44±0.16	0.65±0.15	1.29±0.62	0.43±0.14	0.71±0.34
B.M.	1.25±0.09	5.72±0.29	8.57±0.64	10.34±1.18	12.85±1.64
Tumor	0.31±0.12	2.37±0.14	4.14±0.66	7.84±0.31	5.76±0.40
Feces	0.06±0.03	3.73±0.47	1.53±0.69	2.36±0.75	2.72±0.48
Tumor/muscle	0.7	3.67	3.22	18.16	8.07

per week (Figures 6A and B). The weight loss of each mouse in each group was not less than 20% of the initial value. In terms of tumor growth, compared with the control group, the order of therapeutic efficacy was the combined group ($p<0.01$), and the chemotherapy group ($p<0.01$), followed by the radiotherapy group.

Weight and tumor size tracking during multi-dose therapeutic efficacy assessment. In order to evaluate the efficacy of multi-dose, treatment was started when the tumor size grew to 115 mm^3. During the course of treatment, the body weight and tumor size were assessed twice a week (Figures 6C and D). The weight loss of each mouse in each group was not less than 20% of the initial value. In terms of tumor growth, compared with the control group, the order of efficacy was the combined group ($p<0.01$), and the chemotherapy group ($p<0.05$), followed by the radiotherapy group. Tumor growth delays are listed in Table III, and the combination index was 1.045. The formula is as follows (41):

Combination index = Expected growth inhibition rate/
Mean growth inhibition rate of combine group.

Bioluminescence to track tumor growth as an assessment of therapeutic efficacy. In the established animal model, tumor cells (HT-29/*tk-luc*) were implanted subcutaneously in NOD/SCID mice, and the location and growth of tumors was tracked by the bioluminescence (BLI) produced by the cells. On the 20th day after tumor cell implantation, tumor growth in each mouse was assessed when the tumor size grew to about 100 mm^3. Bioluminescence image tracking was performed twice a week until the end of the treatment process. As shown in Figure 7A, the number of photons was positively correlated with the tumor size, so the size of each group of tumors was successfully traced and accessed by imaging. The ROI of the tumor site is shown in Figure 7B. Obviously, the number of photons detected in the combined group was the lowest, which indicated that the growth of tumor was greatly suppressed in the combination group, followed by the groups of chemotherapy alone and radiotherapy alone. In the control group, tumor growth was not suppressed at all; the highest number of photons per sec were detected. The tumors in the control group were larger than those in any other group. It was obvious that the biological luminescence range was wider, followed by the radiotherapy group, while the chemotherapy and the combined group did not show any difference when observed by naked eye (Figure 7C).

Therapeutic efficacy evaluation with ^{124}I-FIAU micro-PET. At the end of the treatment courses, three mice were taken from each group and were intravenously administered with ^{124}I-FIAU. Since the *tk* gene expressed by tumor cells allows specific FIAU binding to the tumor, micro-PET was performed 24 h after FIAU injection (Figure 8A). The cumulative radioactivity of the combined group was the lowest, which indicated that the growth of tumor was greatly suppressed in the combination group, followed by the groups of chemotherapy alone and radiotherapy alone (Figure 8B). The cumulative radioactivity was positively correlated with the tumor size (Figure 8C).

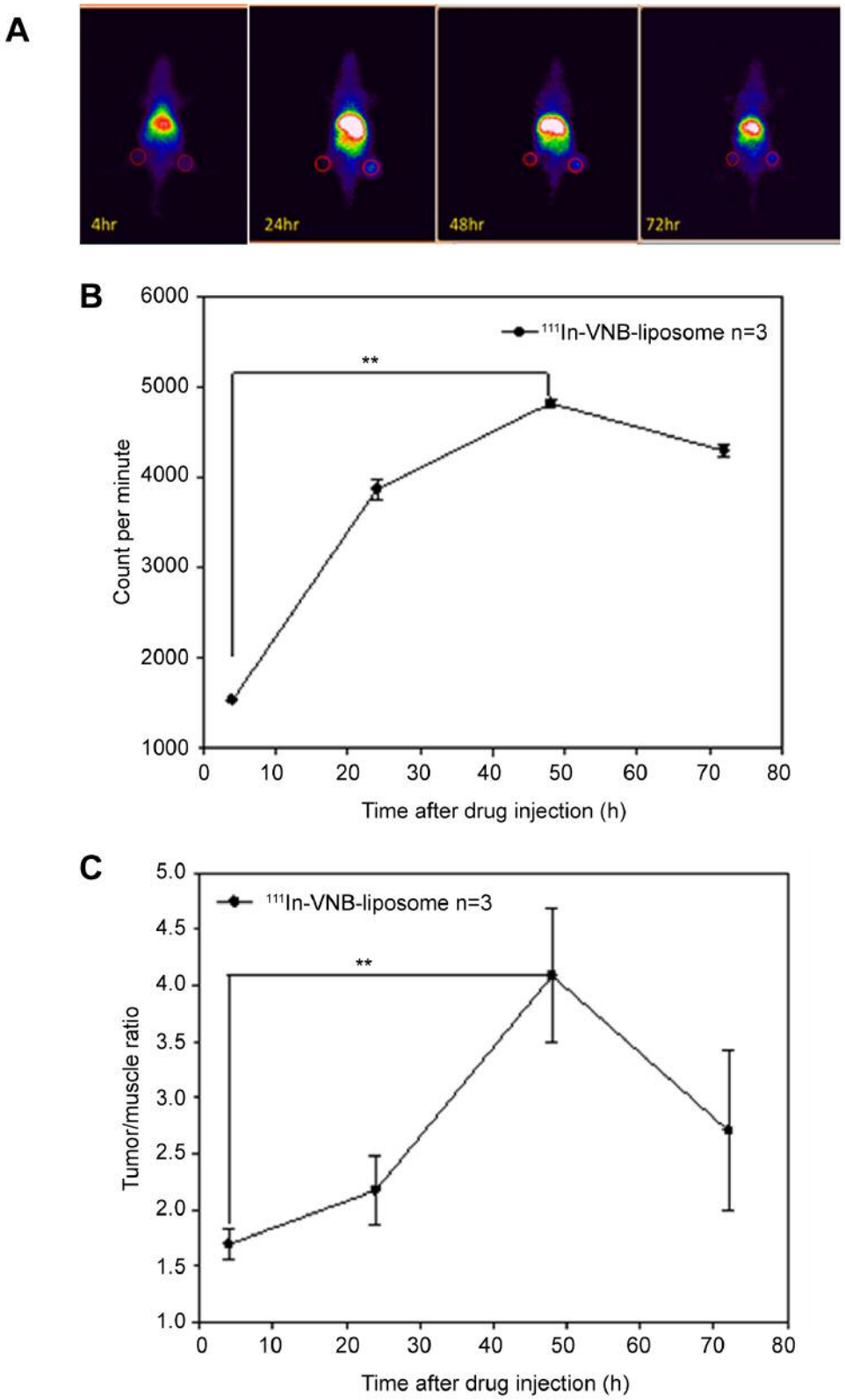

Figure 3. *Detection of liposomes targeted tumor with a γ-camera. (A) The images at 4, 24, 48, and 72 h after the intravenous administration of the drug ^{111}In-VNB-liposomes; (B) The count value at the tumor site by γ-imaging; (C) The ratio of the photon number of the tumor site to the normal tissue by γ-imaging analysis. Data are expressed as mean±SE. *p<0.05, **p<0.01. The experiments were repeated 3 times.*

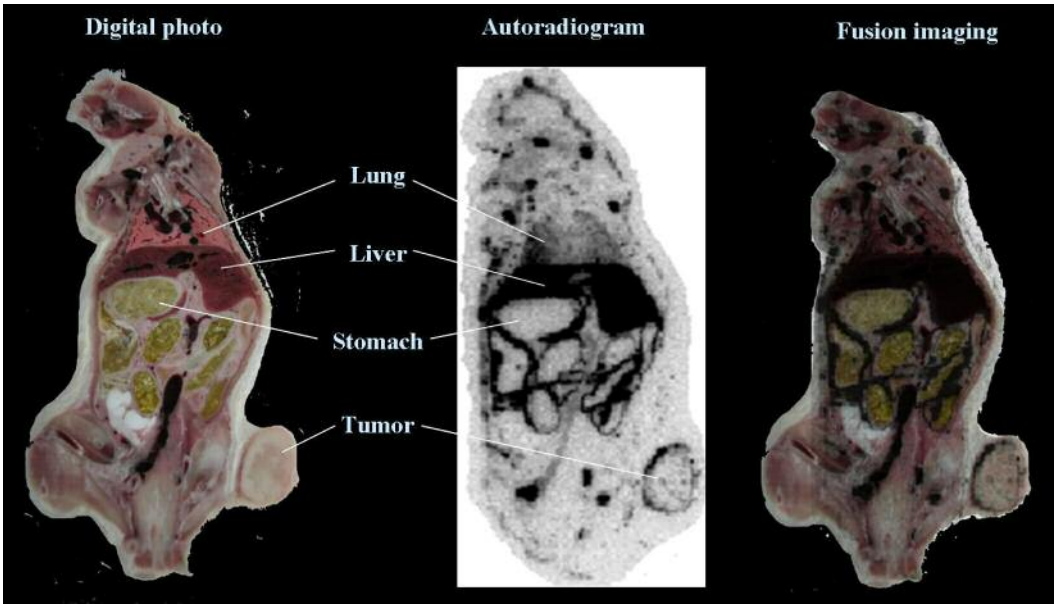

Figure 4. *The mice were subjected to whole-body autoradiography after intravenous injection of ^{111}In-VNB-liposome (100 μCi, 3 mg/kg, 100 μl) for 48 h. Images from left to right are optical images, autoradiographic and fusion images, respectively.*

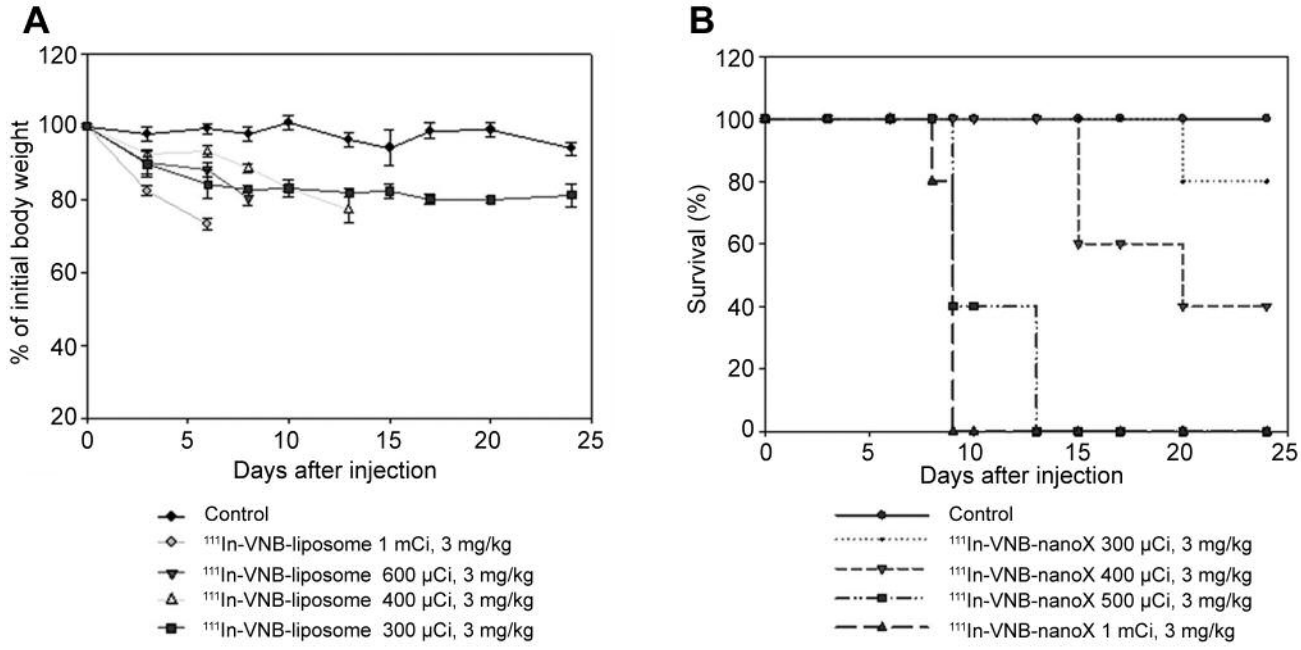

Figure 5. *Maximum tolerated dose of ^{111}In-VNB-liposome in SCID mice. The maximum tolerated dose of the ^{111}In-VNB-liposomes in mice was observed after three weeks of intravenous administration of the drug and the survival of mice. (A) The continuous changes in mouse body weight after administration of the indicated treatments; (B) The survival curve of the mice after administration of the indicated treatments.*

Therapeutic efficacy evaluation with ^{18}F-FEAU micro-PET. At the end of treatment courses, three mice were taken from each group and were intravenously administered with ^{18}F-FEAU. Since the *tk* gene expressed by tumor cells allows specific binding of FEAU to tumor, micro-PET was performed 1 h after FEAU injection (Figure 9A). As in the case of ^{124}I-FIAU, the cumulative radioactivity of the ^{18}F-FEAU plus VNB group was the lowest, which indicated that

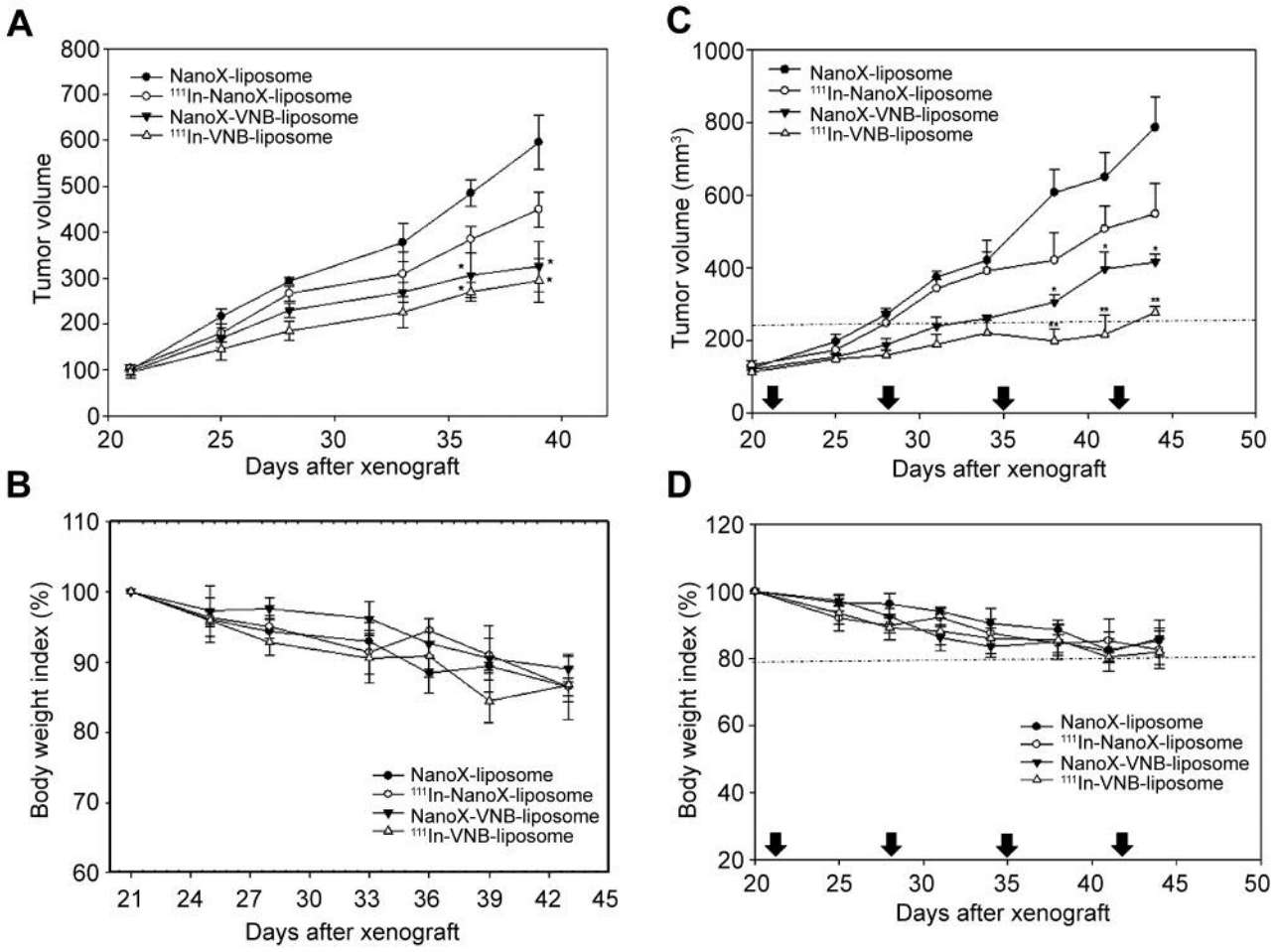

Figure 6. *Weight and tumor size examined following single dose therapeutic efficacy assessment. (A) Tumor growth curve of mice during treatment. Treatment initiated when the tumor grew to about 100 mm^3. Data are expressed as mean±SE. *p<0.05, Student's t-test. The experiments were repeated 3 times; (B) The graph of body weight changes in mice following the indicated treatments; (C) Tumor growth curve of mice following the indicated treatments. Treatment was initiated when the tumor size grew to an average of about 115 mm^3, with the arrow pointing the time of administration. The dividing line is twice as large as the size of the initial tumor treated (about 230 mm^3) and is used as the basis for calculating the number of days of tumor growth inhibition. Data are expressed as mean±SE. *p<0.05, **p<0.01, Arrow indicates the time of the drug injection. The experiments were repeated 3 times; (D) The graph of body weight changes in mice following the indicated treatments. Treatment was initiated when the tumor size grew to an average of about 115 mm^3, with the arrow pointing the time of administration.*

the growth of tumor was greatly suppressed, followed by the groups of VNB alone and ^{18}F-FEAU alone (Figure 9B). The cumulative radioactivity was positively correlated with the tumor size (Figure 9C).

Biochemical analysis of liver and kidney function in mice. At the end of the treatment process and on the 50th day after the tumor was implanted, 5 mice in each group were sacrificed, and their blood was subject to blood biochemical analysis. All groups administered with a liposome-encapsulated drug, whether it was the radiotherapy group, the chemotherapy group, or the combined group, the levels of the liver function indexes alanine aminotransferase (ALT) and aspartate amino-transferase (AST) were both higher than those of normal mice (Table IV). The results indicated that the mice had liver inflammation.

Discussion

The first aim of the current study was the application of a liposome-encapsulated drug delivery system, which can achieve targeted therapy *via* its enhanced permeability and retention (EPR) effects on tumor cells. The diameter of the liposomes was about 100 nm, which is the most suitable size. The liposomes used in this experiment were of 100 nm in their diameter, which has been shown to allow entrance in

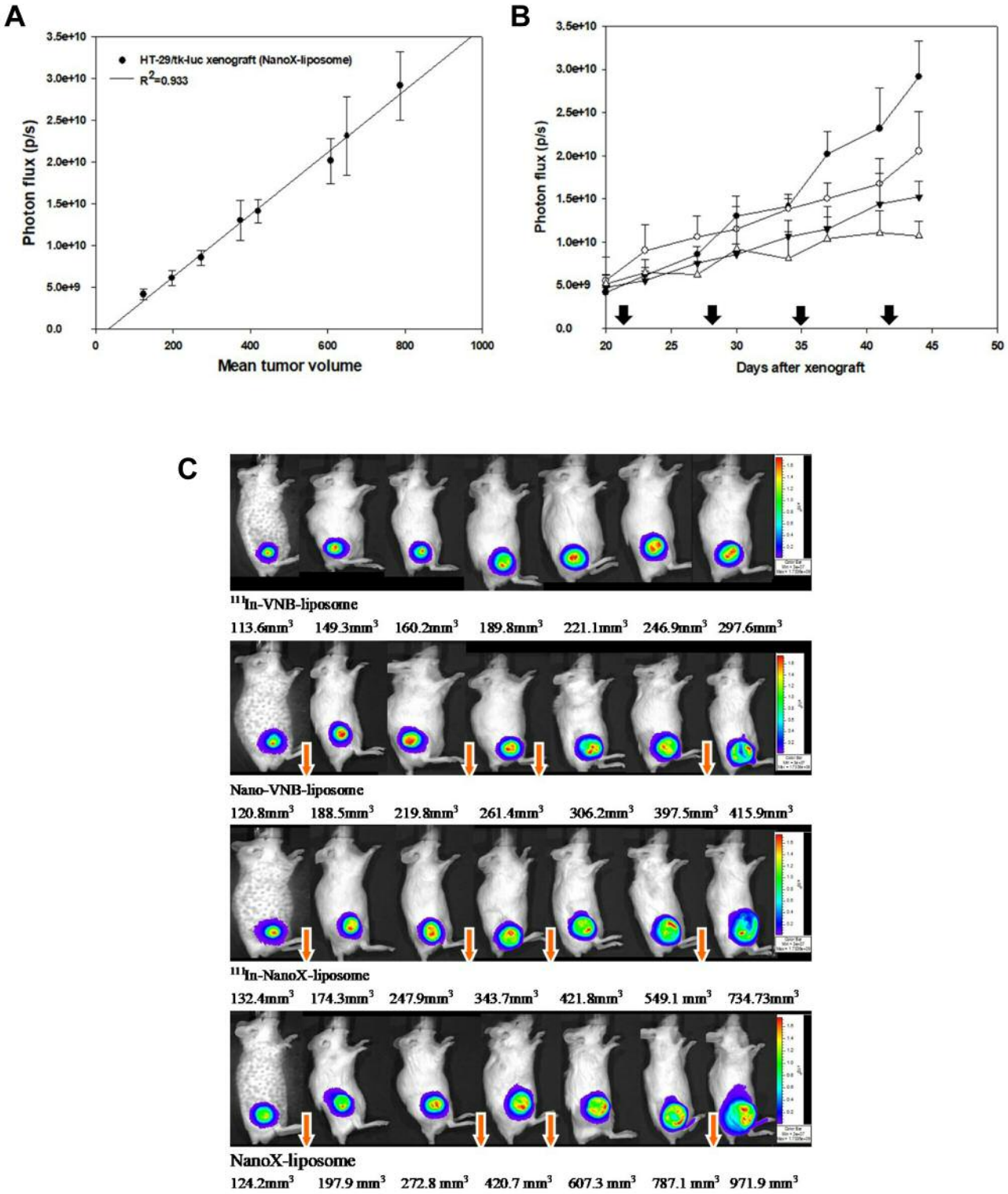

Figure 7. *Bioluminescent tracking of tumor growth in mice. (A) The linear relationship between tumor size and the number of photons emitted with R^2=0.933; (B) Bioluminescence images were used for drug efficacy evaluation; (C) Bioluminescence images of subcutaneous HT-29/tk-luc tumors in NOD/SCID mice. On the 20th day after planting the cells, when the tumor grew to about 100 mm^3, the mice in each group (n=5) were tracked twice a week, until the end of the treatment process. The arrow points the time of administration. Data are expressed as mean±SE. *p<0.05, **p<0.01, The experiments were repeated 3 times.*

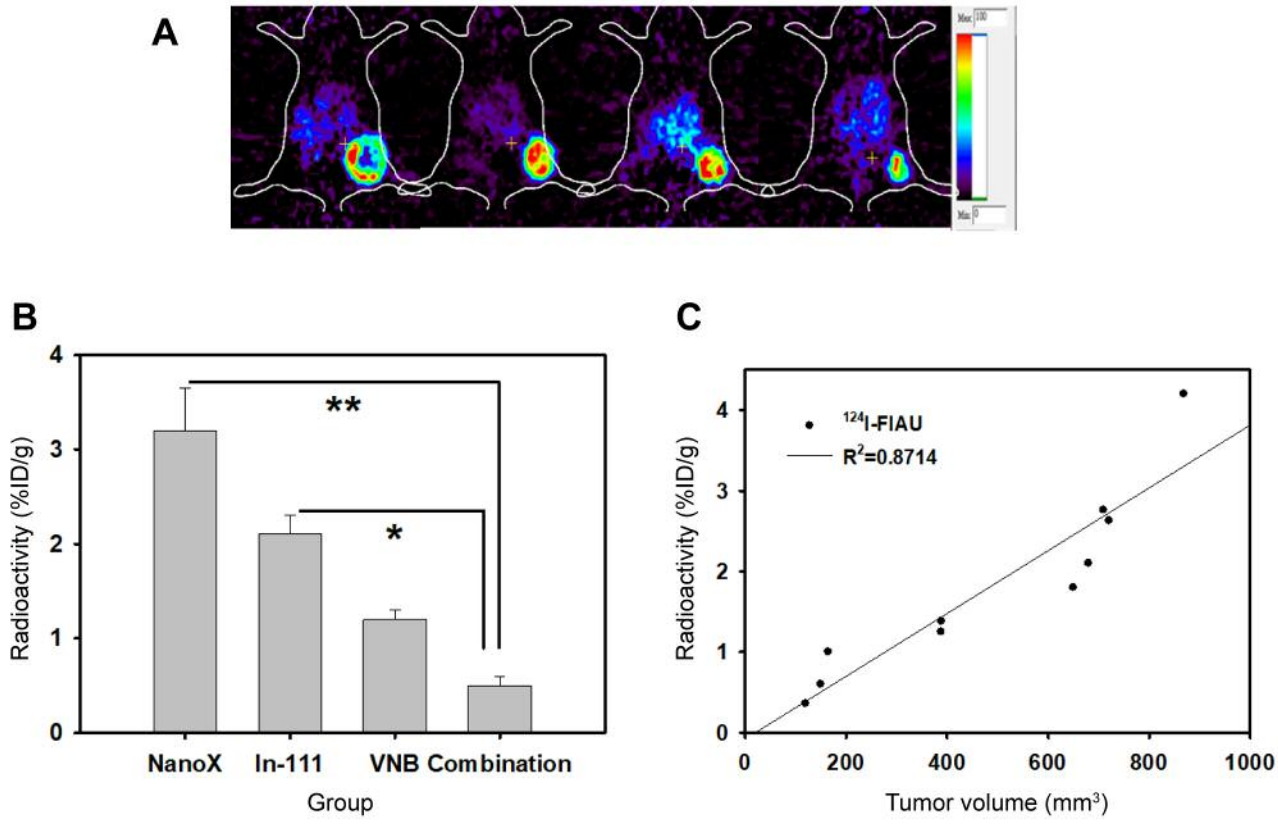

Figure 8. *Evaluation of the therapeutic effect by 124I-FIAU micro-PET. At the end of the treatment period, that is, on the 48th day after tumor implantation, the mice were intravenously injected with the radioactive probe ^{124}I-FIAU which could be metabolized by the herpes simplex virus type 1 thymidine kinase (HSV1-tk) expressed by the tumor cell line to perform micro-PET. (A) The positron tomography images of the control group, the radiotherapy group, the chemotherapy group, and the combined group; (B) Statistical analysis of the results of radioactivity of the tumor sites. Data are expressed as mean±SE. *p<0.05, **p<0.01, The experiments were repeated 3 times; (C) The images of tumors as those shown in (A) were circled as regions-of-interest (ROIs) and quantified as a function of tumor size. A positive correlation was found with R^2=0.8714.*

Table III. *Tumor growth delay and tumor control rate for therapeutic effect evaluation.*

Groups	n/group	Tumor growth delay	Mean growth inhibition rate
Liposome	5	NA	NA
^{111}In-liposome	5	1	0.698
VNB-liposome	5	7	0.528
^{111}In-VNB-liposome	5	16	0.352

the cancer cells *via* endocytosis, delivering the encapsulated drug to them and inducing cytotoxicity (42-45).

The second aim of the study was the application of a molecular imaging system to follow up the biodistribution of the PEG-liposome-encapsulated antitumor drugs. The human reticuloendothelial system and immune cells have been found capable of capturing the circulated liposomes (46) and, at the same time, the biodistribution of these liposome-encapsulated drugs among the organs are very important in clinical practice but not easy to follow-up. In 2007, Papahadjopoulos *et al.*, found that the cumulative amounts of conventional liposomes in the liver and the spleen can reach a significant level at 2 h after intravenous injection, while the amounts of PEG-liposomes were relatively low. It has been hypothesized that PEG-liposomes may reduce the detection of macrophages in the liver and spleen (42).

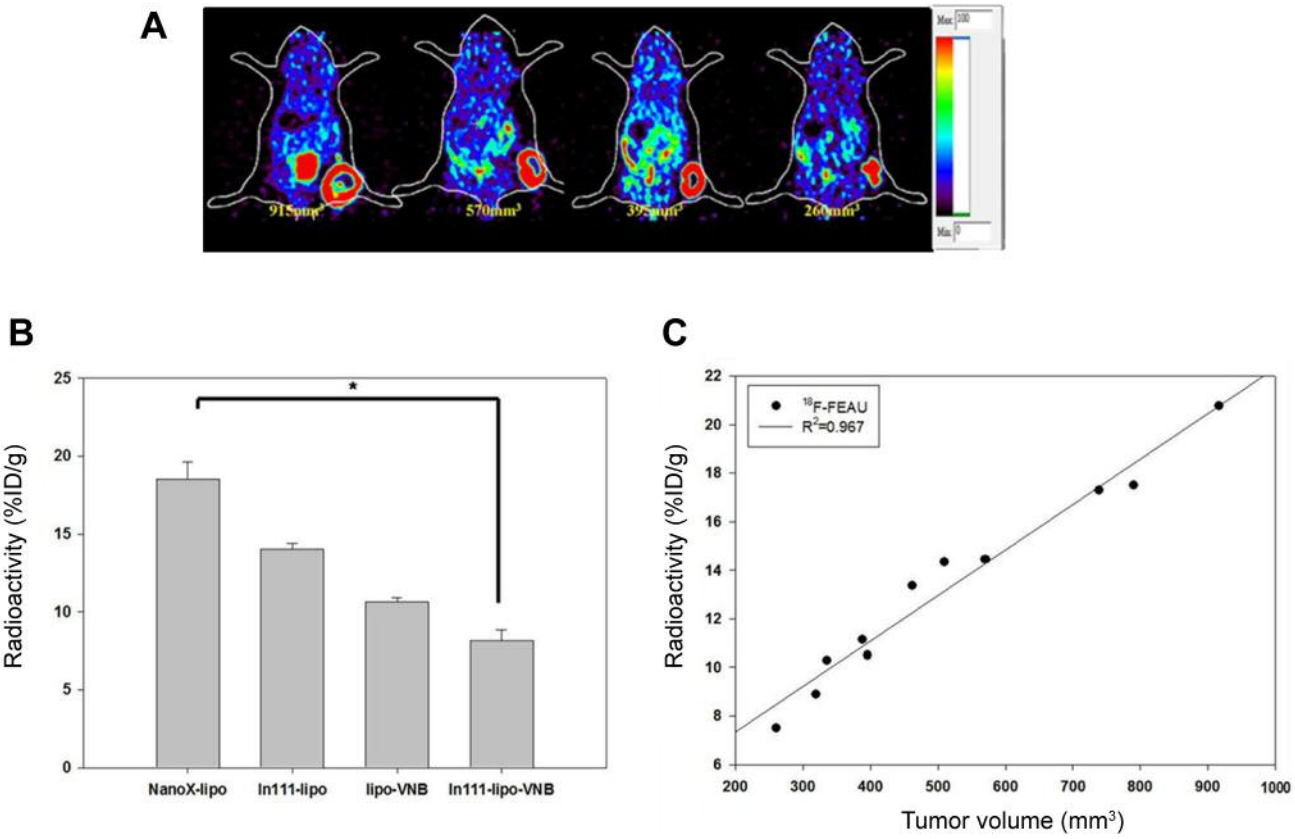

Figure 9. *Evaluation of the therapeutic effect of ^{18}F-FEAU micro-PET. At the end of the treatment process, that is, on the 48th day after tumor implantation, the mice were given intravenous the radioactive probe 18F-FEAU for 1 h and then subjected to micro-PET for 10 min. (A) The positron tomography images of the control group, the radiotherapy group, the chemotherapy group, and the combined group; (B) Statistical analysis of the results of radioactivity of the tumor sites. Data are expressed as mean±SE. *p<0.05, **p<0.01, The experiments were repeated 3 times; (C) The images of tumors as those shown in (A) were circled as regions-of-interest (ROIs) and quantified as a function of tumor size. A positive correlation was found with R^2=0.967.*

Table IV. *Biochemical analysis under the different treatments.*

	Normal	Liposome	^{111}In-liposome	VNB-liposome	^{111}In-VNB-liposome
ALP	118.50±11.95	40.67±4.81	44.00±4.00	37.33±5.81	110.67±56.85
ALT	31.50±4.99	57.67±8.21	164.00±91.28	159.67±118.72	139.67±17.95
AST	315.25±89.35	203.33±39.79	630.33±282.08	614.00±381.00	759.33±215.38
CRE	0.33±0.03	0.27±0.03	0.30±0.06	0.37±0.03	0.37±0.12
BUN	30.93±0.63	27.00±2.87	29.13±4.71	27.80±3.75	25.33±1.32
ALB	2.58±0.11	2.23±0.13	2.23±0.09	2.20±0.12	2.40±0.12

ALP: Alkaline phosphatase; ALT: alanine aminotransferase; AST: aspartate amino-transferase; CRE: creatinine; BUN: blood urine nitrogen; ALB: albumin.

Similarly, Ogawa *et al*. have also found that the biodistribution of PEG-modified ^{111}In-labeled phosphatidyl serine liposomes in the liver was low (47, 48). In the current study, we found that the biodistribution of PEG-liposome was low in the liver and high in the spleen (Figure 1 and Table I). The differential distributions in liver and spleen have also been reported by Lee *et al*. using the same liposome composition (16). In 2009, Chou *et al*. reported that high concentrations of PEG can reduce the uptake of liposomes by reticuloendothelial tissues (24). In 2010's,

radio oncologists have applied radionuclide ^{111}In to bind with liposomes and investigate their biodistribution by molecular imaging, however, these pilot studies had not investigated the cytotoxicity of radionuclides to cancer cells (47-49). ^{111}In is a γ-emitting isotope capable of being tracked by a radio-imaging system and killing cancer cells by inducing DNA double strand breaks (50, 51).

The highlights of the study are that we have not only validated the application of the combination of VNB plus ^{111}In in rodent models (16), but also extended the efficacy of VNB plus ^{111}In by multiple low dose treatments. In 2008, our team loaded liposomes with the radioactive ^{111}In and the chemotherapeutic VNB and compared the therapeutic effects of them with other potential combinations (39). In 2012, the overall efficacies of the ^{111}In-VNB-liposomes were investigated in a rat model with a perfect correlation between the pharmacokinetics and biodistribution (52). In the current study, we made a further modification by reducing the dose of the chemotherapeutic drugs from 5 mg/kg to 3 mg/kg and re-evaluated the overall efficacy from single dose to multiple doses. The multi-dose treatment showed a much better therapeutic effect than the single-dose treatment mode with regard to tumor growth inhibition (Figure 9 and Table III). Although the detail mechanisms and intracellular signaling networks are still largely unknown, our study indicated that the ^{111}In-VNB-liposome could serve as a colorectal cancer therapeutic drug, while the efficacies of multiple low doses were much better than that of a single dose.

Conclusion

Assessing the therapeutic effect of ^{111}In-VNB-liposomes on tumors, we obtained a good pharmacokinetic and biodistribution profile indicating that liposomes are ideal drug carriers for the treatment of cancer. The application of ^{111}In-VNB-liposomes has a synergistic effect in the treatment of colorectal cancer, and its toxicity is within an acceptable range. Most valuably, we have demonstrated that ^{111}In-VNB-liposomes could be administered to rodent models for the treatment of colorectal cancer and can be applied in multiple doses with a lower dose per fraction, *i.e.* smaller fraction size, instead as a single dose of a larger fraction size. Again, we demonstrated that the current multimodalities of an imaging system capable of tracking tumor growth and drug distribution simultaneously is indeed a convenient and powerful evaluating therapeutic system for translating research results in clinical practice in the era of precision and personalized medicine.

Conflicts of Interest

No conflicts of interest exist regarding this study.

Authors' Contributions

Research Design: Chien YC, Chou YH and Hwang JJ; Experiment Performance: Wang WH, Chen CH, Chang WS and Tsai CW; Statistical Analysis: Chien YC and Chou YH; Manuscript Writing: Bau DT and Hwang JJ; Reviewing and Revising: Bau DT, Chang WS and Tsai CW.

References

1 Smith RA, Manassaram-Baptiste D, Brooks D, Doroshenk M, Fedewa S, Saslow D, Brawley OW and Wender R: Cancer screening in the United States, 2015: a review of current American cancer society guidelines and current issues in cancer screening. CA Cancer J Clin *65*: 30-54, 2015. PMID: 25581023. DOI: 10.3322/caac.21261

2 Stewart BW and Wild C: International agency for research on cancer, world health organization. World cancer report, 2014. Available at: https://www.drugsandalcohol.ie/28525/1/World%20Cancer%20Report.pdf

3 Torre LA, Bray F, Siegel RL, Ferlay J, Lortet-Tieulent J and Jemal A: Global cancer statistics, 2012. CA Cancer J Clin *65*: 87-108, 2015. PMID: 25651787. DOI: 10.3322/caac.21262

4 Weinberg BA, Marshall JL and Salem ME: The growing challenge of young adults with colorectal cancer. Oncology (Williston Park) *31*: 381-389, 2017. PMID: 28516436.

5 Wang JL, Chang CH, Lin JW, Wu LC, Chuang LM and Lai MS: Infection, antibiotic therapy and risk of colorectal cancer: a nationwide nested case-control study in patients with Type 2 diabetes mellitus. Int J Cancer *135*: 956-967, 2014. PMID: 24470385. DOI: 10.1002/ijc.28738

6 Jung SY and Zhang ZF: The effects of genetic variants related to insulin metabolism pathways and the interactions with lifestyles on colorectal cancer risk. Menopause *26*: 771-780, 2019. PMID: 30649085. DOI: 10.1097/GME.0000000000001301

7 Jemal A, Thomas A, Murray T and Thun M: Cancer statistics, 2002. CA Cancer J Clin *52*: 23-47, 2002. PMID: 11814064. DOI: 10.3322/canjclin.52.1.23

8 Miller KD, Siegel RL, Lin CC, Mariotto AB, Kramer JL, Rowland JH, Stein KD, Alteri R and Jemal A: Cancer treatment and survivorship statistics, 2016. CA Cancer J Clin *66*: 271-289, 2016. PMID: 27253694. DOI: 10.3322/caac.21349

9 Bartsch R, Wenzel C, Altorjai G, Pluschnig U, Bachleitner-Hoffmann T, Locker GJ, Rudas M, Mader R, Zielinski CC and Steger GG: Results from an observational trial with oral vinorelbine and trastuzumab in advanced breast cancer. Breast Cancer Res Treat *102*: 375-381, 2007. PMID: 17028979. DOI: 10.1007/s10549-006-9342-5

10 Cazzaniga ME, Camerini A, Addeo R, Nole F, Munzone E, Collova E, Del Conte A, Mencoboni M, Papaldo P, Pasini F, Saracchini S and Bocci G: Metronomic oral vinorelbine in advanced breast cancer and non-small-cell lung cancer: current status and future development. Future Oncol *12*: 373-387, 2016. PMID: 26584409. DOI: 10.2217/fon.15.306

11 Ngan VK, Bellman K, Hill BT, Wilson L and Jordan MA: Mechanism of mitotic block and inhibition of cell proliferation by the semisynthetic Vinca alkaloids vinorelbine and its newer derivative vinflunine. Mol Pharmacol *60*: 225-232, 2001. PMID: 11408618. DOI: 10.1124/mol.60.1.225

12 Potier P: The synthesis of Navelbine prototype of a new series of vinblastine derivatives. Semin Oncol *16*: 2-4, 1989. PMID: 2540531.
13 Drugs@FDA: FDA Approved Drug Products n.d. Available at: https://www.accessdata.fda.gov/scripts/cder/daf/
14 Hartimath SV, Alizadeh E, Solomon VR, Chekol R, Bernhard W, Hill W, Parada AC, Barreto K, Geyer CR and Fonge H: Preclinical evaluation of (111)In-Labeled PEGylated maytansine nimotuzumab drug conjugates in EGFR-positive cancer models. J Nucl Med *60*: 1103-1110, 2019. PMID: 30655327. DOI: 10.2967/jnumed.118.220095
15 Chow TH, Lin YY, Hwang JJ, Wang HE, Tseng YL, Pang VF, Liu RS, Lin WJ, Yang CS and Ting G: Therapeutic efficacy evaluation of ^{111}In-labeled PEGylated liposomal vinorelbine in murine colon carcinoma with multimodalities of molecular imaging. J Nucl Med *50*: 2073-2081, 2009. PMID: 19949027. DOI: 10.2967/jnumed.109.063503
16 Lee WC, Hwang JJ, Tseng YL, Wang HE, Chang YF, Lu YC, Ting G, Whang-Peng J and Wang SJ: Therapeutic efficacy evaluation of ^{111}in-VNB-liposome on human colorectal adenocarcinoma HT-29/luc mouse xenografts. Nucl Instruments Methods Phys Res Sect A Accel Spectrometers, Detect Assoc Equip *569*: 497-504, 2006. DOI: 10.1016/j.nima.2006.08.135
17 Allen TM, Hansen CB and deMenezes DEL: Pharmacokinetics of long-circulating liposomes. Adv Drug Deliv Rev *16*: 267-284. DOI: 10.1016/0169-409X(95)00029-7
18 Jha S, Sharma PK and Malviya R: Liposomal drug delivery system for cancer therapy: Advancement and patents. Recent Pat Drug Deliv Formul *10*: 177-183, 2016. PMID: 27712569. DOI: 10.2174/1872211310666161004155757
19 Zylberberg C and Matosevic S: Pharmaceutical liposomal drug delivery: a review of new delivery systems and a look at the regulatory landscape. Drug Deliv *23*: 3319-3329, 2016. PMID: 27145899. DOI: 10.1080/10717544.2016.1177136
20 Woodle MC and Lasic DD: Sterically stabilized liposomes. Biochim Biophys Acta *1113*: 171-199, 1992. PMID: 1510996. DOI: 10.1016/0304-4157(92)90038-c
21 Boerman OC, Storm G, Oyen WJ, van Bloois L, van der Meer JW, Claessens RA, Crommelin DJ and Corstens FH: Sterically stabilized liposomes labeled with indium-111 to image focal infection. J Nucl Med *36*: 1639-1644, 1995. PMID: 7658225.
22 Allen TM and Cullis PR: Liposomal drug delivery systems: from concept to clinical applications. Adv Drug Deliv Rev *65*: 36-48, 2013. PMID: 23036225. DOI: 10.1016/j.addr.2012.09.037
23 Chang CY, Chen CC, Lin LT, Chang CH, Chen LC, Wang HE, Lee TW and Lee YJ: PEGylated liposome-encapsulated rhenium-188 radiopharmaceutical inhibits proliferation and epithelial-mesenchymal transition of human head and neck cancer cells *in vivo* with repeated therapy. Cell Death Discov *4*: 100, 2018. PMID: 30393570. DOI: 10.1038/s41420-018-0116-8
24 Chow TH, Lin YY, Hwang JJ, Wang HE, Tseng YL, Wang SJ, Liu RS, Lin WJ, Yang CS and Ting G: Improvement of biodistribution and therapeutic index *via* increase of polyethylene glycol on drug-carrying liposomes in an HT-29/luc xenografted mouse model. Anticancer Res *29*: 2111-2120, 2009. PMID: 19528471.
25 Emfietzoglou D, Kostarelos K and Sgouros G: An analytic dosimetry study for the use of radionuclide-liposome conjugates in internal radiotherapy. J Nucl Med *42*: 499-504, 2001. PMID: 11337529.
26 Vaage J, Mayhew E, Lasic D and Martin F: Therapy of primary and metastatic mouse mammary carcinomas with doxorubicin encapsulated in long circulating liposomes. Int J Cancer *51*: 942-948, 1992. PMID: 1639542. DOI: 10.1002/ijc.2910510618
27 Petersen AL, Henriksen JR, Binderup T, Elema DR, Rasmussen PH, Hag AM, Kjaer A and Andresen TL: *In vivo* evaluation of PEGylated (6)(4)Cu-liposomes with theranostic and radiotherapeutic potential using micro PET/CT. Eur J Nucl Med Mol Imaging *43*: 941-952, 2016. PMID: 26646780. DOI: 10.1007/s00259-015-3272-6
28 Ogawara K, Un K, Minato K, Tanaka K, Higaki K and Kimura T: Determinants for *in vivo* anti-tumor effects of PEG liposomal doxorubicin: importance of vascular permeability within tumors. Int J Pharm *359*: 234-240, 2008. PMID: 18448289. DOI: 10.1016/j.ijpharm.2008.03.025
29 Maruyama K: Intracellular targeting delivery of liposomal drugs to solid tumors based on EPR effects. Adv Drug Deliv Rev *63*: 161-169, 2011. PMID: 20869415. DOI: 10.1016/j.addr.2010.09.003
30 Kibria G, Hatakeyama H, Sato Y and Harashima H: Anti-tumor effect *via* passive anti-angiogenesis of PEGylated liposomes encapsulating doxorubicin in drug resistant tumors. Int J Pharm *509*: 178-187, 2016. PMID: 27234700. DOI: 10.1016/j.ijpharm.2016.05.047
31 Johnson M, Karanikolas BD, Priceman SJ, Powell R, Black ME, Wu HM, Czernin J, Huang SC and Wu L: Titration of variant HSV1-tk gene expression to determine the sensitivity of ^{18}F-FHBG PET imaging in a prostate tumor. J Nucl Med *50*: 757-764, 2009. PMID: 19372484. DOI: 10.2967/jnumed.108.058438
32 Lee O, Kim J and Oh C: Small-animal PET imaging analysis with [(18) F]FHBG in a mouse model of HSV1-tk gene expression in melanoma. Exp Dermatol *27*: 199-201, 2018. PMID: 29197132. DOI: 10.1111/exd.13475
33 Liang L, Bi W, Chen W, Lin Y and Tian Y: Combination of MPPa-PDT and HSV1-TK/GCV gene therapy on prostate cancer. Lasers Med Sci *33*: 227-232, 2018. PMID: 29306975. DOI: 10.1007/s10103-017-2331-6
34 Li H, Li JZ, Helm GA and Pan D: Non-invasive imaging of firefly luciferase reporter gene expression using bioluminescence imaging in human prostate cancer models. Biotechnol Appl Biochem *46*: 179-184, 2007. PMID: 17073822. DOI: 10.1042/BA20060081
35 Marques SM and Esteves da Silva JC: Firefly bioluminescence: a mechanistic approach of luciferase catalyzed reactions. IUBMB Life *61*: 6-17, 2009. PMID: 18949818. DOI: 10.1002/iub.134
36 Brennan TV, Lin L, Huang X and Yang Y: Generation of luciferase-expressing tumor cell lines. Bio Protoc *8*: e2817, 2018. PMID: 29963584. DOI: 10.21769/BioProtoc.2817
37 Falcone L and Casucci M: Exploiting secreted luciferases to monitor tumor progression *in vivo*. Methods Mol Biol *1393*: 105-111, 2016. PMID: 27033220. DOI: 10.1007/978-1-4939-3338-9_10
38 Tseng YL, Hong RL, Tao MH and Chang FH: Sterically stabilized anti-idiotype immunoliposomes improve the therapeutic efficacy of doxorubicin in a murine B-cell lymphoma model. Int J Cancer *80*: 723-730, 1999. PMID: 10048974. DOI: 10.1002/(sici)1097-0215(19990301)80:5<723::aid-ijc16>3.0.co;2-l
39 Chow TH, Lin YY, Hwang JJ, Wang HE, Tseng YL, Pang VF, Wang SJ, Whang-Peng J and Ting G: Diagnostic and therapeutic evaluation of ^{111}In-vinorelbine-liposomes in a human colorectal carcinoma HT-29/luc-bearing animal model. Nucl Med Biol *35*: 623-634, 2008. PMID: 18589307. DOI: 10.1016/j.nucmedbio.2008.04.001

40 Chen LC, Chang CH, Yu CY, Chang YJ, Hsu WC, Ho CL, Yeh CH, Luo TY, Lee TW and Ting G: Biodistribution, pharmacokinetics and imaging of (188)Re-BMEDA-labeled pegylated liposomes after intraperitoneal injection in a C26 colon carcinoma ascites mouse model. Nucl Med Biol *34*: 415-423, 2007. PMID: 17499731. DOI: 10.1016/j.nucmedbio.2007.02.003

41 Morgillo F, Kim WY, Kim ES, Ciardiello F, Hong WK and Lee HY: Implication of the insulin-like growth factor-IR pathway in the resistance of non-small cell lung cancer cells to treatment with gefitinib. Clin Cancer Res *13*: 2795-2803, 2007. PMID: 17473213. DOI: 10.1158/1078-0432.CCR-06-2077

42 Papahadjopoulos D, Allen TM, Gabizon A, Mayhew E, Matthay K, Huang SK, Lee KD, Woodle MC, Lasic DD and Redemann C: Sterically stabilized liposomes: improvements in pharmacokinetics and antitumor therapeutic efficacy. Proc Natl Acad Sci USA *88*: 11460-11464, 1991. PMID: 1763060. DOI: 10.1073/pnas.88.24.11460

43 Maeda H, Wu J, Sawa T, Matsumura Y and Hori K: Tumor vascular permeability and the EPR effect in macromolecular therapeutics: a review. J Control Release *65*: 271-284, 2000. PMID: 10699287. DOI: 10.1016/s0168-3659(99)00248-5

44 Asadi N, Davaran S, Panahi Y, Hasanzadeh A, Malakootikhah J, Fallah Moafi H and Akbarzadeh A: Application of nanostructured drug delivery systems in immunotherapy of cancer: a review. Artif Cells Nanomed Biotechnol *45*: 18-23, 2017. PMID: 27196810. DOI: 10.1080/21691401.2016.1178136

45 Mi Y, Shao Z, Vang J, Kaidar-Person O and Wang AZ: Application of nanotechnology to cancer radiotherapy. Cancer Nanotechnol *7*: 11, 2016. PMID: 28066513. DOI: 10.1186/s12645-016-0024-7

46 Sun X, Yan X, Jacobson O, Sun W, Wang Z, Tong X, Xia Y, Ling D and Chen X: Improved tumor uptake by optimizing liposome-based RES blockade strategy. Theranostics *7*: 319-328, 2017. PMID: 28042337. DOI: 10.7150/thno.18078

47 Ogawa M, Umeda IO, Kosugi M, Kawai A, Hamaya Y, Takashima M, Yin H, Kudoh T, Seno M and Magata Y: Development of ^{111}In-labeled liposomes for vulnerable atherosclerotic plaque imaging. J Nucl Med *55*: 115-120, 2014. PMID: 24337605. DOI: 10.2967/jnumed.113.123158

48 Ogawa M, Uchino R, Kawai A, Kosugi M and Magata Y: PEG modification on (111)In-labeled phosphatidyl serine liposomes for imaging of atherosclerotic plaques. Nucl Med Biol *42*: 299-304, 2015. PMID: 25533763. DOI: 10.1016/j.nucmedbio.2014.12.004

49 Lamichhane N, Dewkar GK, Sundaresan G, Mahon RN and Zweit J: [(18)F]-fluorinated carboplatin and [(111)In]-liposome for image-guided drug delivery. Int J Mol Sci *18*: 1079, 2017. PMID: 28524076. DOI: 10.3390/ijms18051079

50 Mariani G, Bodei L, Adelstein SJ and Kassis AI: Emerging roles for radiometabolic therapy of tumors based on auger electron emission. J Nucl Med *41*: 1519-1521, 2000. PMID: 10994732.

51 Hindie E, Zanotti-Fregonara P, Quinto MA, Morgat C and Champion C: Dose deposits from ^{90}Y, 177Lu, ^{111}In, and ^{161}Tb in micrometastases of various sizes: Implications for radiopharmaceutical therapy. J Nucl Med *57*: 759-764, 2016. PMID: 26912441. DOI: 10.2967/jnumed.115.170423

52 Lee WC, Chang CH, Huang CM, Wu YT, Chen LC, Ho CL, Chang TJ, Lee TW and Tsai TH: Correlation between radioactivity and chemotherapeutics of the (111)In-VNB-liposome in pharmacokinetics and biodistribution in rats. Int J Nanomedicine *7*: 683-692, 2012. PMID: 22359447. DOI: 10.2147/IJN.S28279

Received September 30, 2019
Revised November 4, 2019
Accepted November 5, 2019